Improving detection of surface discontinuities in visual–force control systems

J. Pomares , P. Gil , G.J. García , J.M. Sebastián , F. Torres

Physics, Systems Engineering and Signal Theory Department, University of Alicante, PO Box 99, 03080 Alicante, Spain
DISAM, Polytechnic University of Madrid, Cl José Gutiérrez Abascal, 2, 28006 Madrid, Spain

Abstract

In this paper, a new approach to detect surface discontinuities in a visual–force control task is described. A task which consists in tracking a surface using visual–force information is shown. In this task, in order to reposition the robot tool with respect to the surface it is necessary to determine the surface discontinuities. This paper describes a new method to detect surface discontinuities employing sensorial information obtained from a force sensor, a camera and structured light. This method has proved to be more robust than previous systems even in situations where high frictions occur.

Keywords: Surface discontinuity recognition; Visual–force fusion; Visual robot guidance

1. Introduction

Nowadays, visual servoing systems guide a robot by using image information obtained from an object observed by an eye-in-hand or eye-to-hand camera system In applications such as interaction with unknown workspaces, the image information must be combined with that obtained from other sensors in order to improve the system behaviour. Additional sensorial information can be integrated in the visual loop like that obtained from a laser. By attaching a structured light emitter to the camera, it is possible to project visual marks onto the object surface which can be used in the control loop in order to position the camera located at the end-effector. an image-based visual servoing approach based on structured light for plane-to-plane positioning is proposed. other works related with the joint use of visual information and structured light are described.

However, in manipulation applications in which the robot interacts with its workspace, force sensor data must be jointly used with the information obtained from the camera in order to control not only the robot position but also the interaction with the contact surface. Furthermore, a great number of approaches employed to fuse visual–force information have been developed. Most of these approaches are based on hybrid control. Within these approaches we should mention studies which extend the "task frame" formalism a system to grasp objects in real time is described. It uses information from an external camera and that obtained from the force sensors of a robotic hand. Another strategy used for the combination of both sensorial systems is the use of impedance control. Based on the basic scheme of impedance control, we should mention several modifications like the one described which adds an external control loop that consists of a visual controller which generates the references for an impedance control system. the use of virtual forces applied to approaching tasks without contact is proposed. In addition, vision-force control techniques for robot systems with unknown contact surface have been proposed in the literature In order to improve the

robustness of these systems we have combined image and force information in order to detect discontinuities in unknown surfaces.

Our previous works have shown the necessity of maintaining the coherence between the control actions obtained from the visual force sensors in order to guarantee that these control actions will not be contradictories. To do so, it is necessary to modify the image trajectory tracked by the visual servoing system so that the new trajectory is coherent with the contact surface. Furthermore, if a change in the surface occurs, the new surface must be recognized. In this paper, we are not interested in developing a surface recognition method (to do so, our previous algorithms are employed). However, this paper describes a robust method to detect changes in the contact surface employing a multisensorial system composed of an eye-in-hand camera system, a force sensor and a laser.

This paper is organized as follows: the visual force control system to track surfaces is first described in Section 2; Section 3 shows a method based on the Generalized Likelihood Ratio (obtained from the interaction forces) to detect surface discontinuities; in Section 4, a strategy to determine surface discontinuities in the image space based on structured light is presented; Section 5 describes the joint use of the two previous methods in order to obtain a robust estimation of the surface discontinuity; in Section 6, experimental results, using an eye-in-hand camera system, confirm the validity of the proposed algorithms; the final section presents the main conclusions arrived at.

2. Tracking surfaces using force and visual servoing

In this section the method to track surfaces using visual force information is described. The objective of the impedance control is to carry out the combined control of the robot motion and their interaction force. The following impedance equation enforces an equivalent mass-damper-spring behaviour for the pose when the end-effector exerts a force $\boldsymbol{F}$ on the environment:

$$\boldsymbol{F} = \mathbf{I}_F \Delta\ddot{\boldsymbol{x}}_{ve} + \mathbf{D}_F \Delta\dot{\boldsymbol{x}}_{ve} + \mathbf{K}_F \Delta\boldsymbol{x}_{ve} \tag{1}$$

where $\boldsymbol{x}_c$ is the current end-effector pose, $\boldsymbol{x}_v$ is the reference trajectory, $\Delta\boldsymbol{x}_{ve} = \boldsymbol{x}_v - \boldsymbol{x}_c$ ($\Delta\dot{\boldsymbol{x}}_{ve}$ and $\Delta\ddot{\boldsymbol{x}}_{ve}$ are the first and the second time derivative repectively), $\mathbf{I}_F \in \Re^{nxn}$ is the inertial matrix, $\mathbf{D}_F \in \Re^{nxn}$ is damping matrix and $\mathbf{K}_F \subset \Re^{nxn}$ is the stiffness. They are diagonal matrices and characterize the desired impedance function.

To implement the controller, we have chosen a position-based impedance control system called accommodation control in which the desired impedance is limited to pure damping $\mathbf{D}$ (the main aspects of the stability of this type of control is shown). In this case:

$$\boldsymbol{F} = \mathbf{D}\Delta\dot{\boldsymbol{x}}_{ve} \tag{2}$$

Therefore, the control law obtained is:

$$\dot{\boldsymbol{x}}_c = \dot{\boldsymbol{x}}_v - \mathbf{D}^{-1}\boldsymbol{F} \tag{3}$$

where the term $\dot{\boldsymbol{x}}_v$ is obtained from the visual loop. The visual servoing system carries out the tracking of the desired trajectory in the image space. To do this, an image-based control scheme to regulate to value 0 the following vision-based task function is used

$$\boldsymbol{e} = \widehat{\mathbf{J}}_I^+ \cdot (\mathbf{s} - \mathbf{s}_d(t)) \tag{4}$$

where $\mathbf{s} = [f_1, f_2, \ldots, f_M]^T$ are the features extracted from the image, $\widehat{\mathbf{J}}_I^+$ is an estimation of the pseudoinverse of the interaction matrix and $\mathbf{s}_d(t)$ is the desired trajectory in the image. To carry out the tracking of the trajectory, the following velocity must be applied to the robot (with respect to the coordinate frame located at the eye-in-hand camera):

$$\dot{\boldsymbol{x}}_v = -\lambda_V \cdot \boldsymbol{e} + \widehat{\mathbf{J}}_I^+ \cdot \frac{\partial \mathbf{s}_d(t)}{\partial t} \tag{5}$$

where $\lambda_V > 0$ is the gain of the proportional controller.

3. Detecting surface discontinuities from interaction forces

To assure that a given task in which it is required an interaction with the setting is correctly developed, the system must carry out a variation of the trajectory in the image, which depends on the spatial restrictions imposed by the interaction forces. Therefore, given a collision with the setting and having recognized the normal vector of the contact surface [11], the transformation $\mathbf{T}_r$ that the camera must undergo to fulfil the spatial restrictions is determined. This transformation is calculated so that it represents the nearest direction to the one obtained from the image-based control system, and is also contained in the plane of the surface. Thus, we guarantee that the visual information will be coherent with the information obtained from the force sensor.

In our previous studies we have shown a method to detect discontinuities on an interaction surface based on the GLR (Generalized Likelihood Ratio) This method has several possible problems (i.e., false detections) and a more extensive study is shown in this paper. However, several aspects of this approach are highlighted in order to demonstrate the detections problems. Previously, the GLR has been applied in other environments such as the 2-D motion estimation in an image sequence and the detection of discontinuities of road curvatures

In order to reduce the peak-to-peak noise level when the robot is tracking a surface, the interaction forces are filtered using a Kalman filter whose main equations are:

$$^{k+1}x = \mathbf{F} \cdot {}^{k}x + {}^{k}v \tag{6}$$

$$^{k}z = \mathbf{H} \cdot {}^{k}x + {}^{k}w \tag{7}$$

where:

- $^{k}x \subset \Re^n$ is the state vector.
- ^{k}z is the measurement vector.
- $\mathbf{F}$ is the transition state matrix, which relates the state in the previous step $k-1$ to the current state k without noise.

- **H** is the measurement matrix, which relates the state to the measurement ${}^{k}z$.
- We assume that the random variables ${}^{k}v$ and ${}^{k}w$ are independent and have a normal distribution, i.e., $p(v) \sim N(0,\mathbf{Q})$, $p(w) \sim N(0,\mathbf{R})$ (the values of **Q** and **R** are experimentally determined and are considered to be 10^{-5} and 10^{-2}, respectively).

The state model will be:

$$ {}^{k+1}\boldsymbol{F} = \mathbf{I} \cdot {}^{k}\boldsymbol{F} + {}^{k}v \tag{8} $$

where $\boldsymbol{F}$ are the interaction forces as described in the previous section.

The vector $\boldsymbol{F}$ has 6 components (linear forces and moments). We define the binary vector a with 6 components (one for each component of vector $\boldsymbol{F}$). A given component has value 1 if the system tries to detect changes in the corresponding direction (0 if the system does not detect changes in this direction). The innovation ${}^{k}\gamma$ considered in the filter is:

$$ {}^{k}\gamma = {}^{k}\gamma_{n} + g(k;\theta) \cdot \alpha \tag{9} $$

where:

- ${}^{k}\gamma_{n}$ represents the innovation which will be obtained if there is no change (${}^{k|k-1}x$ is the prediction of the state vector):

$$ {}^{k}\gamma_{n} = {}^{k}z \quad \mathbf{H} \cdot {}^{k|k-1}x \tag{10} $$

- $g(k;\theta)$ is the effect (on the innovation measured at the iteration k) of the change in the surface that is produced at the iteration θ, in the direction of the change a.
- α is the size of the hypothetical change in the magnitude of the force.

$j(k;\theta)$ is the effect of the change in the surface over the innovation value. The change is produced at iteration θ and is measured at iteration k. It is supposed that the change occurs in the indicated direction by a. If $\theta < k$, the following values can be obtained:

$$ \begin{aligned} g(k;\theta) &= a - j(k-1;\theta) \\ j(k;\theta) &= \mathbf{F} \cdot j(k-1;\theta) + {}^{k}\mathbf{K} \cdot g(k;\theta) \end{aligned} \tag{11} $$

In the following equations we consider a system to detect changes in the interval $k \quad \xi < \theta < k$. The value of ξ is established high enough to compensate the noise effect in the signal. In filtering interaction forces, we have obtained good results with $\xi = 10$. The test function to determine a change in the interaction forces filtered in the direction a is:

$$ l(k;\theta) = \frac{d^2(k;\theta)}{c(k;\theta)} \tag{12} $$

where:

$$ c(k;\theta) = \sum_{j=\theta}^{k} \frac{g^2(j;\theta)}{{}^{j}v} \tag{13} $$

and:

$$ d(k;\theta) = \sum_{j=\theta}^{k} \frac{g(j;\theta) \cdot {}^{j}\gamma}{{}^{j}v} \tag{14} $$

The value of the $l(k;\theta)$ increases when abrupt changes are determined from the obtained interaction forces. Therefore, the greater the $l(k;\theta)$ the greater the probability of a change in the surface. We have defined the threshold U so that if $l(k;\theta) > U$ then a change in the surface is produced (empirically, this threshold has been established at 1000).

In Fig. 1, the values of the force f_z and the GLR obtained during the tracking of two curved surface are shown. This method is not robust enough to detect the exact point in which a discontinuity in the surface occurs. For example, in Fig. 1b there are three different moments in which the discontinuity is detected ($l(k;\theta)$ is greater than 1000). As this figure shows, false detections can be obtained when high frictions are measured. Furthermore, these false detections can be obtained in other situations due to the high noise level in the measured signal from the force sensor. Therefore, we conclude that this method is only adequate to obtain a value about the probability of a discontinuity in the surface. However, to improve the robustness in the detection, some additional information must be applied.

In the next section, a method based on structured light is defined in order to be combined with the one proposed in this section. The aim is to obtain a robust method for the detection of discontinuities in contact surfaces.

4. Structured light to detect discontinuity zones in the image space

In this section, a new approach, used jointly with the previous section, to detect discontinuity zones in surfaces is proposed. This approach is based on patterns of structured light which are projected on the surfaces of the scene objects. The light beam projection over the different surfaces determines certain discontinuities due to the change of direction of the projection planes. The three-dimensional object features such as depth values and surface orientations produce a different reflectance-distribution function and, therefore, different projection planes. The system employed for the detection process is composed of a CCD camera, a laser LASIRIS SNF with a wavelength of 660 nm, a power of 20 mW, a fan angle about 15° and 7 concentric circles with an interbeam angle of 0.77°. This laser is located next to the camera in the robot end-effector. In this way, the camera-laser system scans the scene in each position executed by the robot.

When more than one light plane hit the different surfaces (i.e., surfaces with different orientations or different

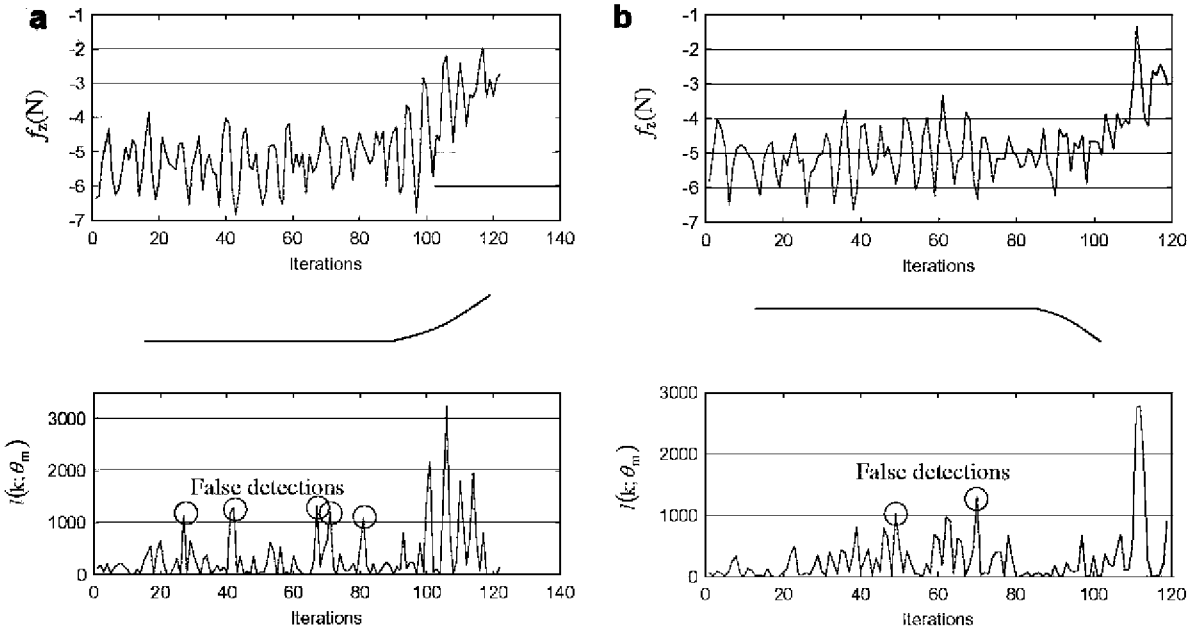

Fig. 1. Evolution of f_z, outline of the surface and parameter $l(k;\theta_m)$ in the tracking of two different surfaces.

depth value of a same object, or surfaces of different objects) a discontinuity effect is observed in the projection planes. The discontinuity is caused by the breakage of light beam projection. Thus, several projection planes displaced in the space can be observed. This can be seen in our study

The pattern employed consists of concentric circles. We have chosen the concentric representation because with parallel lines it is difficult to detect discontinuities of surfaces in polyhedral geometric pieces. These are the type of pieces used in our experiments (Fig. 2a).

In this section, the proposed process for detecting discontinuities using structured light laser is presented.

4.1. Step 1. Detection of beam contour

Once the beam is projected over the objects surface, the first stage consists of extracting the contours of circle pattern. To do so, a Gaussian smoothed process with a 3×3 size mask is firstly employed to reduce the produced noise when the beam hits reflecting surfaces.

Later, the image is binarized by means of a suitable threshold, according to the wavelength of the laser. Experimentally, a saturation threshold about 70 has been considered for 660 nm.

Fig. 3 shows RGB and HSV decomposition to separate an image captured into its RGB and HSV components. When the decomposition is RGB, it creates three greyscale images containing the red, green and blue channels of the image. In this Fig. 3a, it can be observed that only the red colour component contributes most information about the laser beam rather pattern than the rest of colour components (green and blue). The reason for this is that the laser light emitted is coherent. This means that the laser light is a very pure colour. In this case a wavelength of 660 nm determines a pure red colour. A pure colour means

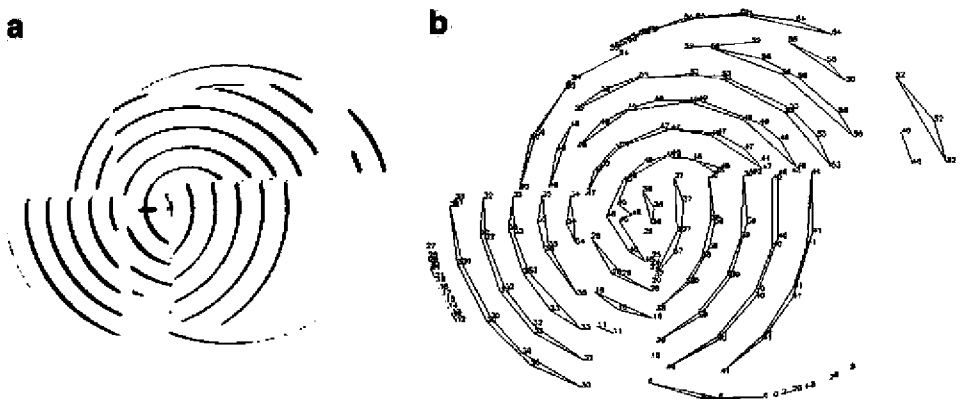

Fig. 2. (a) Projection of the beam on a surface. (b) Approximation of the beam by poly-lines.

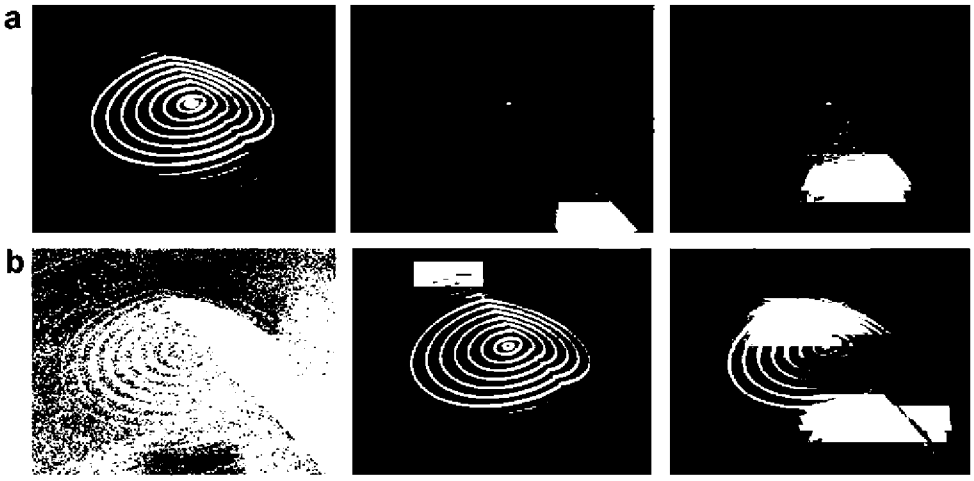

Fig. 3. (a) RGB Decomposition: red, green, blue. (b) HSV decomposition: hue, saturation and luminance values of the image.

a single frequency, which implies narrow peaks in its spectrum lighting graphs. Furthermore, for HSV decomposition, three greyscales are also created, but now they represent the hue, saturation, and value components of the image. So, in Fig. 3b shows that the saturation component offers the best information to recognize the laser beam pattern.

Now, it is necessary to determine what component is more stable and robust to illumination changes: saturation (Fig. 4) or red (Fig. 5). Thus, the influence of each component saturation in order to fix a suitable threshold to extract the contour of the laser beam pattern is shown in Fig. 4.

Fig. 4 shows that a threshold of 70 is the most suitable to extract the saturation. Furthermore, the hue component seems not useful in segmenting the laser beam pattern as it is shown in Fig. 3b. The reason for this is that the hue component does not have a standard linear order. However, if the hue component is ordered with a distance function between the hue values and a reference value (the distance to red colour value) and in addition, the saturation component is used to choose the hue values depending on the saturation values, the hue can be used to extract the contour of the laser. This is shown in Fig. 4b.

In contrast, Fig. 5 shows that the red component is not suitable to fix a threshold to extract the contour of the laser beam pattern. In this case, the visible light has radiations in the range of wavelengths in air [380–750 nm] and the red emitted by the laser is 660 nm. Fig. 5 shows that the threshold below 155 is not valid to extract the contour because it has lost information.

If the histogram of the red and the saturation components are studied (Fig. 6), it can be observed that the saturation is more suitable to fix a threshold more robust to changes in the lighting environment. The threshold is fixed in $U = 70$. But also, it is important to emphasize that the HSV model has been used instead of HSI, due to the fact that the saturation component is unstable in others models like HIS, in which pixels with the same visual appearance have a different saturation value.

With this threshold it is possible to extract only the information of contours from the projected laser pattern. Afterwards, these contours are slightly skeletized with a Gaussian filter to reduce the thickness of the circle projections of the beam (Fig. 2a). An alternative could have been to use the morphological filter based on erosion to better the contour of the projection of the beam but the computation time could rise. An excessive smoothed process can produce a loss of information. The points which form the

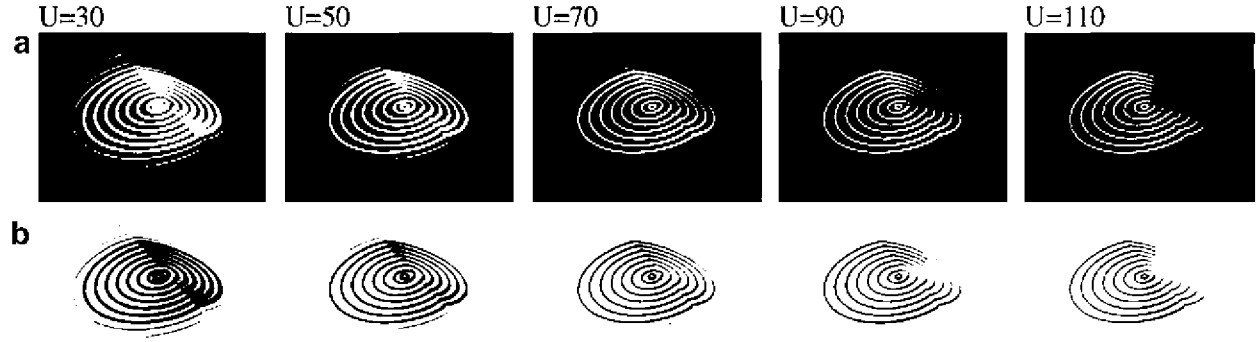

Fig. 4. (a) Influence of thresholding in saturation component. (b) Influence of thresholding in hue component using distance to red colour.

Fig. 5. Influence of thresholding in the red component.

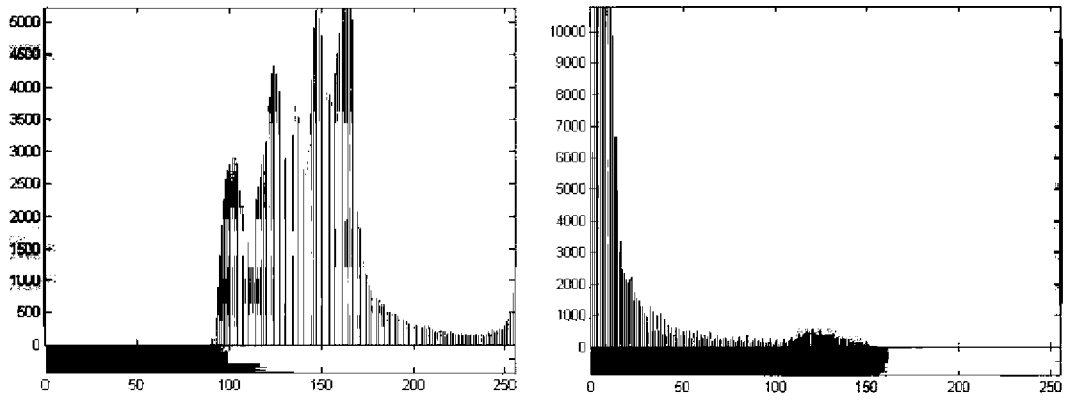

Fig. 6. Influence of thresholding in red component.

contour can be reduced, and furthermore false discontinuities can also appear.

Next, to make the contour detection, the pixels which compose the projected circles in the image are detected by means of a convolution process. In this process, 8-connectivity masks are used Thus, the pixels of boundary which determine each contour are found. This set of pixels corresponds to the 2D-points which compose each projected circle. These pixels are retrieved as edge point by a variant based on the Suzuki algorithm This type of representation in which the curve is coded as a sequence of points is often a good choice because it avoids ambiguity and run very fast in binary images.

4.2. Step 2. Approximation of beam contours

Once the contours have been detected, like a set of points, it is necessary to approximate every contour by means of some kind of geometric primitive which defines those contours using several parameters. These parameters will be employed below in order to differentiate contours. Thus, each circular contour is represented by a polygonal approach. The advantages of a polygonal approach are: on the one hand, obtaining a simple representation for each contour that permits a fast and efficient comparison process between contours; on the other hand, the reduction of the number of "interest points" (points that make up each boundary) detected during the contour extraction process. Thus, the beam projection is only represented by a minimum set of "interest points" without loss of stability in the contour extraction process (Fig. 2b).

Our approach method is based on the Douglas Peucker's algorithm Each contour is approximated by a poly-line, P_s. A contour is defined as a sequence of n points so that $C_s = \{p_1, p_2, \ldots, p_n\}$, and a poly-line P_s can be defined as the union of 1-degree segments, where l denotes each segment.

$$P_s = \cup_{i=1}^{n-1}\{l_i l_{i+1}\} = \cup_{i=1}^{n-1}\{tp_i + (1 \quad t)p_{i+1}/0 \leqslant t \leqslant 1\} \quad (15)$$

$$P_s = \{p_1 \ldots p_n/n \geqslant 2\} \quad (16)$$

The adjustment is based on the representation of a set of points by means of edge segments where the proximity of each point to the edge segment must be inferior to a tolerance factor ε used as reference threshold. The proximity is measured like a normal distance vector to each candidate edge segment.

The algorithm begins approximating all the points of a contour, $C_s = \{p_1, p_2, \ldots, p_n\}$, with a poly-line which joins the first and the last point of the edge contour, $P_s = l_1 = \{p_1 p_n\}$. The distance of each intermediate point to the poly-line is measured, and the farthest point with a tolerance greater than the ε value is added to the simplification process and takes part to build a new poly-line $P_s = \{p_1 p_i p_n\}$. Later, this one is divided into two segments $l_1 = \{p_1 p_i\}$ and $l_2 = \{p_i p_n\}$ and the union of both will compose $P_s = \{l_1, l_2\} = \{p_1 p_i p_n\}$.

Thus, these steps are repeated iteratively for each edge contour until all the points which belong to the poly-line do not violate the value rank marked by the tolerance factor. If the distance of an intermediate point to a poly-line does not exceed the tolerance factor, it is not taken into account for the simplification process of the poly-line.

The polygonal adjustment process allows the approximation of the laser beam contours in a more stable way than a set of contour points. Now, each edge contour is composed by fewer points. Each contour is a set of points greater than two which is the minimum number of points necessary to define a segment.

Nevertheless, in spite of the previous smoothing preprocessing, during the contour detection process, some contours have been approximated by poly-lines of small length. These poly-lines are formed by a small number of points. This fact can be due to noise. These poly-lines do not provide relevant information because their contour points represent small and disposable discontinuities. Therefore, the approximated contours should be filtered in order to work only with those have a certain length so that they are determined by a number of points greater than three $P_s = \{p_1 p_2, \ldots, p_n / n \geqslant 3\}$. Once the previous process has been carried out, it is necessary to label with a number the candidate contours again, disposing those which are not useful because they do not contribute with important discontinuity information or because they can cause confusion (Fig. 7).

4.3. Step 3. Clustering and discontinuity directions

First, the poly-lines with relevant information are chosen, that is only the poly-lines which fulfil the equation $P_s = \{p_1 p_n / n \geqslant 3\}$. Second, the end points of each poly-line with number of points greater than three are selected. The poly-lines are selected because each poly-line is composed by a points set. The points of each poly-line are counted to eliminate the poly-lines composed by less than three points. Afterwards, the maximum distances among points of each poly-line determine the end points in each case. These directions of discontinuity are the zones of breakage of the light beam projections when the beam hits over two surfaces with different depth or orientation.

Later, a method for the adjustment of the "tactically important points" (end points that make up each poly-line) is applied by means of straight lines. These straight lines determine the candidate zones and the suitable direction for the search of possible discontinuities which are present in the surface changes.

A clustering process of "tactically important points" is carried out to determine whichever straight lines are necessary to fit them, and to discriminate what "tactically important points" belong to one or another direction of discontinuity. The clustering process permits to group the "tactically important points" according to two parameters: inertial moments and metric distances Thus, each edge contour approximated by a poly-line P_s has two "tactically important points", each of which must belong to different clusters, and must have associated the central moments of the poly-line to which they belong. The central moments, $\mu_{p,q}$, are invariant to displacements of identical beams in the image, and do not depend on the position that the beam projections have in the image.

$$\mu_{p,q} = \int \int (x - x_c)^p (y - y_c)^q f(x,y) \mathrm{d}x \mathrm{d}y \tag{17}$$

where:

- (x_c, y_c) is the coordinate of the centre of the image $f(x,y)$.
- (x,y) is the position of a point into the image.

Furthermore, it is possible to determine the rotation ϕ of each edge contour around its gravity center from the central moments and with the aid of the components of inertial tensor, as:

$$\phi = \frac{1}{2} \arctan \frac{2\mu_{1,1}}{\mu_{2,0} - \mu_{0,2}} \tag{18}$$

The parameter of inertial moments is employed to discern between "tactically important points" which belong to poly-lines, and therefore to contours with the same orientation. In this way, we have assumed that the beam projections over the same surface of an object A have similar inertial moments. However, in an object B which is overlapping and occluding part of the surface of A, the inertial moments estimated from the beam projections over a surface of B are different to those estimated from A (Fig. 7). When a discontinuity is detected, an orientation change of the beam projections takes place, and a new value of the inertial moments is consequently obtained.

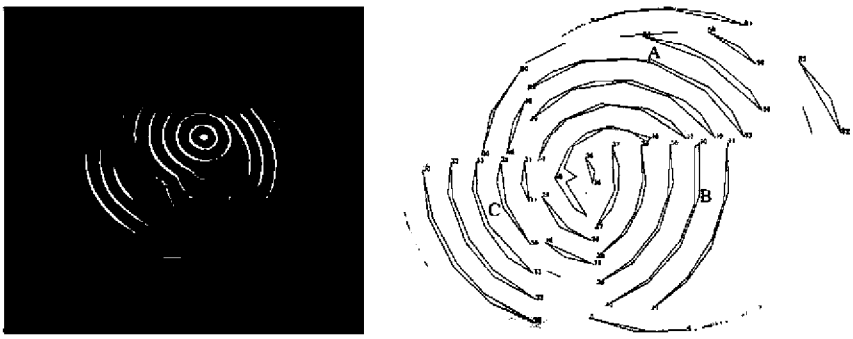

Fig. 7. Distribution of "tactically important points" which define poly-lines obtained by approximation of the beam.

Also, another parameter to highlight is the distance of Minkowski L_2. Thus, the distance of each "tactically important point" to the rest of "tactically important points",d_{L_r}, is calculated, trying to minimize it. In the first step, the square triangular matrix $D_{mxm} = \{V_{p1}, \ldots, V_{pm}\}$ which defines the set of distances among points is made. Each matrix row, V_{pi}, represents the distance, d_{L_r}, among a point p_i and the rest of points. Next, the points which compose each set V_{pi} are ordered. The minimum element, $\min(d_{L_r})$ is calculated as the smallest element of each set V_{pi}.

$$d_{L_r} = \left(\sum_{i,j} |p_i - p_j|^r \right)^{1/r} \tag{19}$$

The distance parameter is used to avoid to group as points of a same discontinuity. Those points can have the same inertial moments, but due to their little proximity they may not belong to the same candidate zone. For this reason, only the "tactically important points", near them and whose poly-lines have similar inertial moments, are clusterized. Then, we obtain n sets of points of the following type: $V_{pi} = \{s_1\ s_2 \ldots s_n\} / \ 0 < i < n$ where $\{s_1\ s_2 \ldots s_n\}$ are the points nearer p_i ordered according to proximity. Finally, the difference of moments for each set of points is obtained as mentioned above.

$$d\phi_{ij} = |\phi_{V_{pi}} - \phi_{V_{sj}}| \tag{20}$$

In this equation the operator |.|define the absolute value. Thus, the distance between two angles is computed as the difference between their absolute value.

From the distances and the difference of moments calculated for each set $V_{pi} = \{s_1 s_2, \ldots, s_n\}$, the clustering process is made. In this way, for any two points p_i and s_j, these will be able to be jointly stored and included in the same cluster. If they fulfill that $d\phi_{ij} < \varphi_c$, with φ_c the angular tolerance allowed so they can be considered as points with similar orientation.

Finally, after the "tactically important points" have been grouped by means of the clustering process, (Fig. 8a), the candidate zones which represent discontinuities in the image are defined as those zones which contain each cluster. In order to determine the search direction of those candidate zones and their boundary it is necessary to make a linear adjustment by least-squares method. This method calculates the straight line segments which diminish the Minkowski's distance $L_1 - L_2$ of each set of "tactically important points" to the straight line segment (Fig. 8b).

5. Robust multisensorial system to detect changes in surfaces

In Section 4, a method to estimate discontinuity zones of a given surface in the image space has been shown. This method provides a line where the discontinuity occurs. Furthermore, in Section 3, a method to detect these

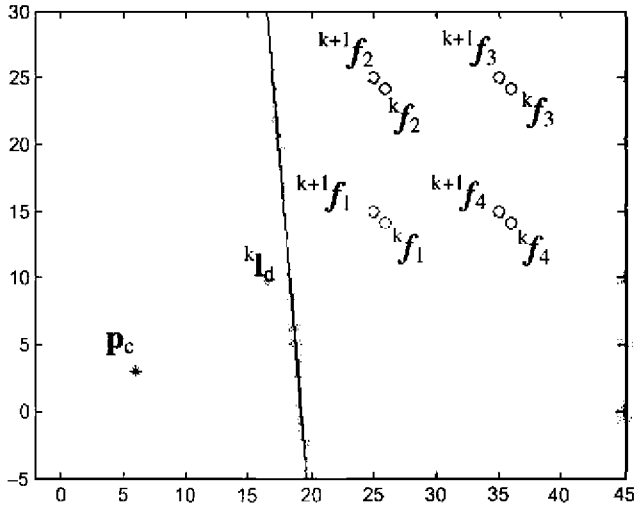

Fig. 9. Features extracted in the image and discontinuity line $^k l_d$.

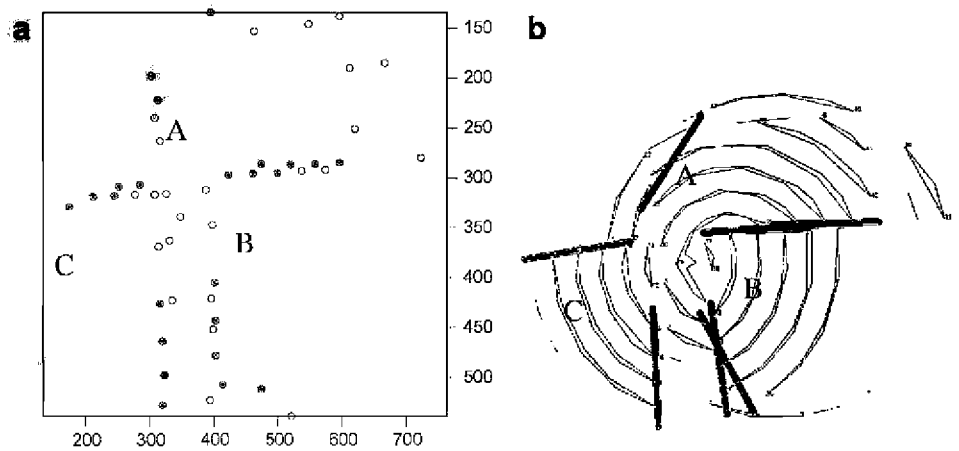

Fig. 8. (a) Clustering process to group the tactically important points that determine directions of discontinuities. (b) Direction of discontinuities by linear fit.

discontinuities based on interaction forces is described. However, both methods independently are not sufficiently robust to detect with high precision the moment in which the surface changes. To avoid the limitation of both sensors this section describes the use of both sensors jointly. To do so, structured light is employed to determine discontinuity zones in which the method described in Section 3 is applied. In this way, the probability of having a false detection is reduced to a minimum.

When the system described in Section 4 based on structured light determines a discontinuity zone, a line is obtained in the image space. This line, ${}^0\mathbf{l}_d$, represents the discontinuity. As Fig. 9 shows, from the visual information it is possible to determine not only the visual features employed by the visual servoing system, but also the point, $\mathbf{p}_c$, in which the end-effector tool collides with the surface. Therefore, the algorithm described in Section 3 will be activated at the moment when $\mathbf{p}_c$ arrives at the discontinuity line ${}^0\mathbf{l}_d$. In this way, false detections are avoided. The estimation of the iteration at which the point $\mathbf{p}_c$ is near the straight line ${}^0\mathbf{l}_d$ is the object of this section.

Once the line ${}^0\mathbf{l}_d$ is detected, its position in future iterations is estimated using information about the position of the features in the image obtained by the visual servoing system. In a certain iteration, the current position of the features, ${}^k\mathbf{s}$, is obtained from the camera, and the desired position of the features, ${}^{k+1}\mathbf{s}$, is obtained from the function $\mathbf{s}_d(t)$ described in Section 2. Using this information, the homography matrix relating these two positions, $\mathbf{G}_k$, can be calculated as it is described in [24]. Fig. 9 shows the current, ${}^k f_i$, and the desired position, ${}^{k+1}f_i$, of the visual features at a certain iteration of the visual servoing task, where i represents the i-th feature extracted from the image.

Once the homography matrix is computed, it is possible to locate in the following iteration $k+1$ the straight line ${}^0\mathbf{l}_d$ obtained with the algorithm described in Section 4. To do so, two points located on the line ${}^k\mathbf{l}_d$ are considered. As these two points are located on the same plane that the features ${}^k f_i$, applying the Eq. (21), the position of each point is determined from the homography matrix $\mathbf{G}_k$ previously obtained:

$$ {}^m\boldsymbol{x}_{k+1} = \mathbf{G}_k {}^m\boldsymbol{x}_k, \quad m = \{1,2\} \tag{21} $$

where ${}^m\boldsymbol{x}_k$ indicates the coordinates of the m-th point in the image at the current iteration and ${}^m\boldsymbol{x}_{k+1}$ are the coordinates of the same point in the image after the camera motion is applied. By calculating the motion of these two points, the position of the virtual line ${}^{k+1}\mathbf{l}_d$ in the image plane can be reconstructed.

The algorithm computes the position of the straight line ${}^i\mathbf{l}_d$ at each iteration of the visual control task until the end-effector of the robot, $\mathbf{p}_c$, is near this line. At this moment, the algorithm described in Section 3 is employed to determine with precision the exact point in which the discontinuity occurs. Fig. 10 shows the simulation of the computed position of the virtual line ${}^0\mathbf{l}_d$ during the visual servoing task. The end-effector, $\mathbf{p}_c$, has a fixed position in the image plane (there is a constant distance between it and the camera). The initial position is indicated by ${}^0\mathbf{l}_d$. The lines represented as ${}^i\mathbf{l}_d$ are the successive estimations obtained by the algorithm described in this section. Finally, the line represented by ${}^f\mathbf{l}_d$ represents the one obtained at the iteration, in which the algorithm detects that the tool connected at the end-effector of the robot is satisfactorily close to this line. At this point, the method described in Section 3 is activated.

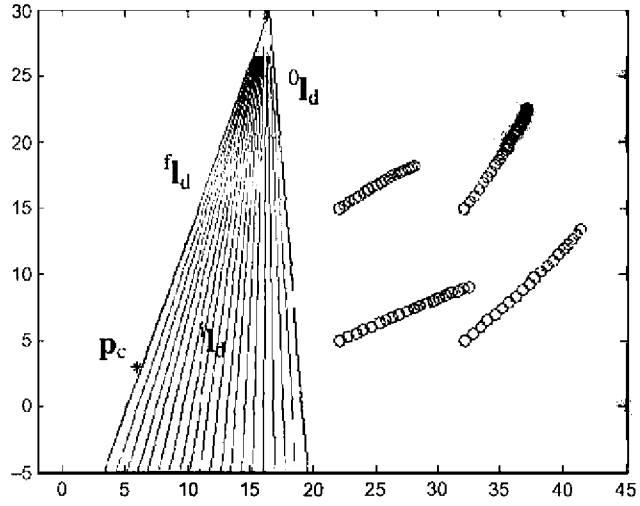

Fig. 10. Projection of the discontinuity during the visual servoing task.

6. Results

6.1. System architecture

The system architecture is composed of an eye-in-hand PHOTONFOCUS camera in the end-effector of a 7 d.o.f. Mitsubishi PA-10 robot (see Fig. 11), which is also equipped with a force sensor (67M25A-I40 from JR3, Inc.) and a laser LASIRIS SNF with a wavelength of

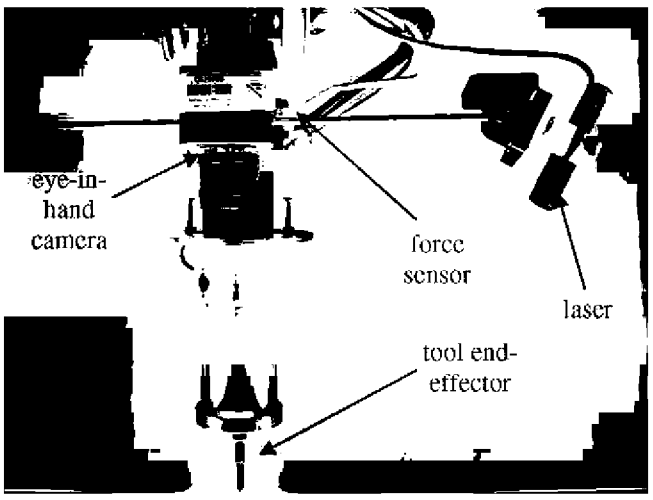

Fig. 11. Experimental setup.

660 nm. A Coreco X64CL-Pro card is used as the image acquisition and processing board. The camera is able to acquire and to process up to 100 frames/s using an image resolution of 320 × 240. In this paper, we are not interested in image processing issues. Therefore, the image trajectory is generated by using four grey marks. The centres of gravity of these marks will be the extracted features.

6.2. *Improving the detection using the multisensorial system*

Now, an experiment in which frictions are generated during the tracking of the surface is described. The discontinuity of the surface is shown in Fig. 12. The interaction forces and the parameter $l(k;\theta)$ obtained in the tracking of the surface using the approach described in Section 3 are shown in Fig. 13. We can observe that the system is able to detect the discontinuity zone, but there are also some false discontinuities detections. To improve the system behaviour the next step is to limit the zones where the discontinuity can appear by using the method based on structured light described in Section 4. Using this method, the discontinuity zone represented by two straight lines in Fig. 14a is obtained. The last step is to determine when the end-effector is located near the discontinuity zone so that the algorithm described in Section 3 is only executed in this zone. This avoids more false detections. Following the process described in Section 5, once the discontinuity line is detected $\mathbf{l}_d$, the homography matrix, $\mathbf{G}_k$, is determined at each iteration of the visual servoing task. This matrix is determined to project the position of the discontinuity line at each iteration, ${}^k\mathbf{l}_d$. Therefore, when this line is sufficiently near to the position of the end-

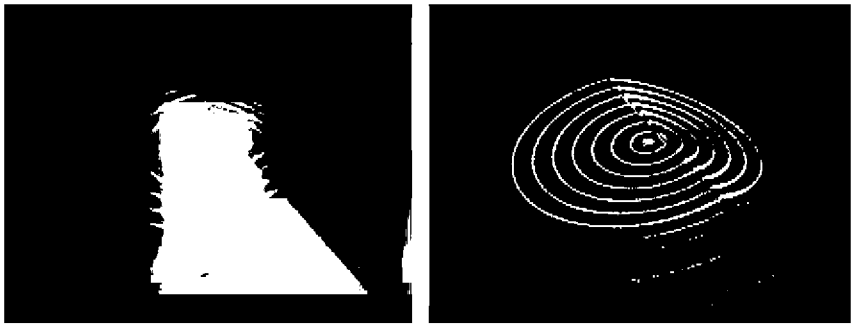

Fig. 12. View of surface discontinuity from laser-camera. Experiment 1.

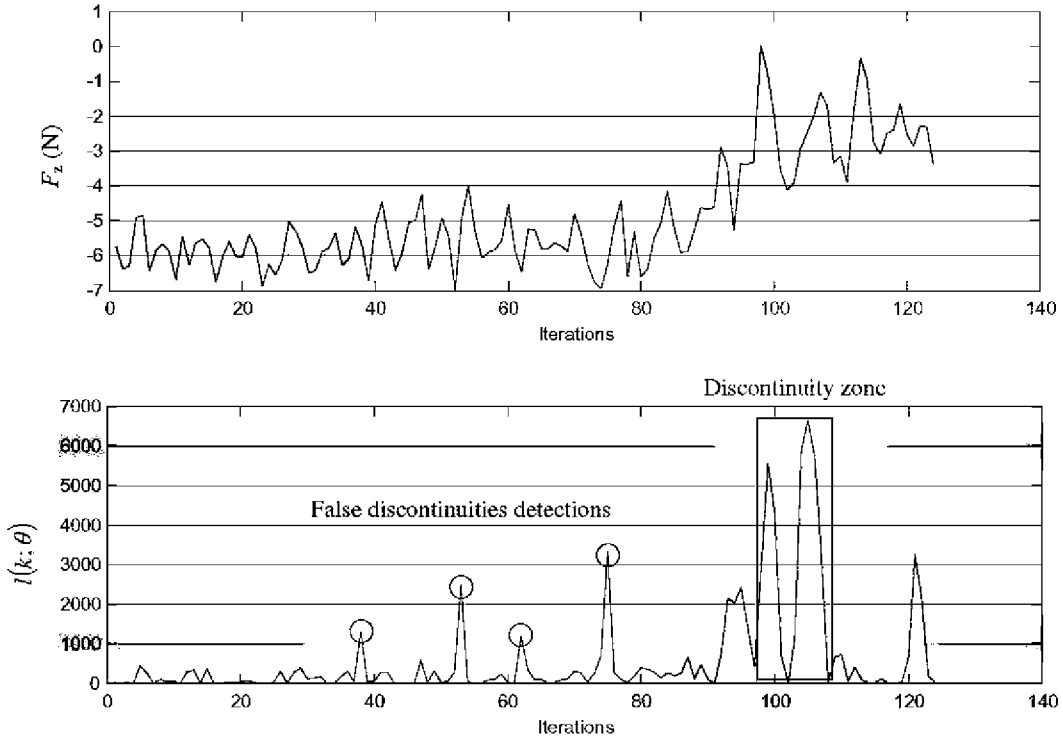

Fig. 13. Interaction forces and values of $l(k;\theta)$ during the tracking of a surface with a discontinuity. Experiment 1.

effector, the algorithm described in Section 3 is executed to determine the exact point of the discontinuity (this process is illustrated in Fig. 14b).

6.3. Improving the detection using the multisensorial system. Experiment 2

In this new experiment, the system is tested in the tracking of the surface shown in Fig. 15. In the experiment shown in Section 6.2, the robot interacts with a convex surface while tracking the desired image trajectory. In this new experiment, the surface presents a concave discontinuity as Fig. 15 shows. The forces measured from the force sensor and the parameter $l(k;\theta)$ obtained in the tracking of the surface are shown in Fig. 16. The discontinuity zone is segmented using the method proposed in Section 4. Fig. 17a shows this discontinuity zone, which is represented by two straight lines. To ensure a more precise and robust detection of the discontinuity, these two lines are projected in the control loop's successive iterations. To do so, the method proposed in Section 5 is used. Therefore, as Fig. 17b shows, the system is able to precisely determine the moment when the tool located at the end-effector of the robot is near the discontinuity zone. In this moment, the system based on the interaction forces described in Section 3 is able to obtain the new discontinuity zone avoiding the false detections.

7. Conclusions

In this paper, a new method to fuse sensorial information obtained from a computer vision system with that obtained from a force sensor has been described. The method was applied to a task which consists of crossing a surface. In this application, it is not only necessary to obtain desired features in the image, but also a tracking of the desired trajectory of the features (fulfilling the desired spatial restrictions) is necessary for the correct tracking to be carried out.

Furthermore, in this paper, a method to detect surfaces discontinuities in visual–force control tasks is described. To do so, first, we have shown an approach to detect these discontinuities by only using force information. However, these approaches are sensitive to

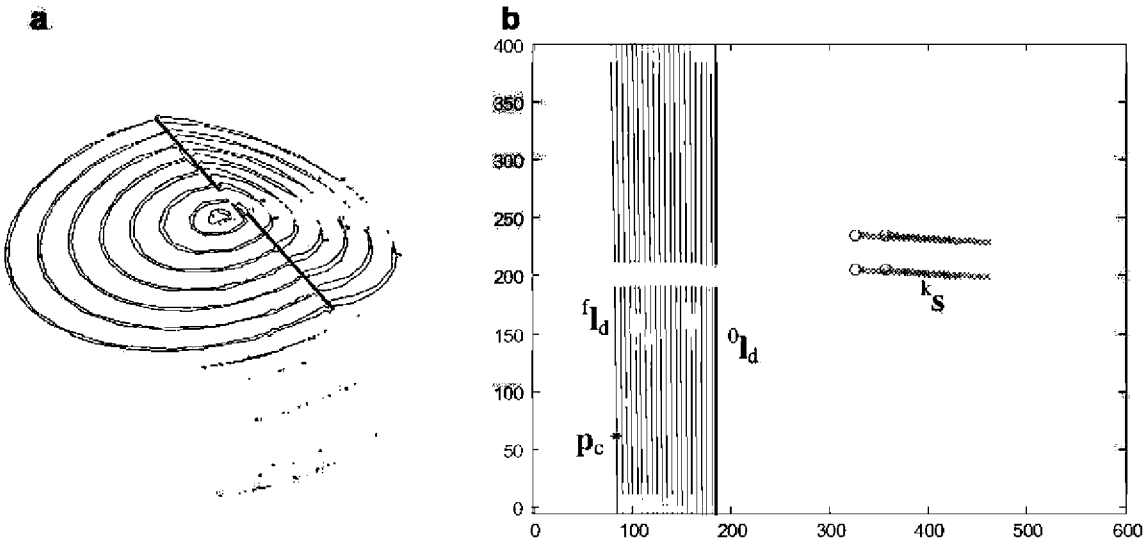

Fig. 14. (a) Zone of discontinuity using the method described in Section 4. (b) Process carried out to determine the point in which the end-effector arrives to the discontinuity. Experiment 1.

Fig. 15. View of surface discontinuity from laser-camera. Experiment 2.

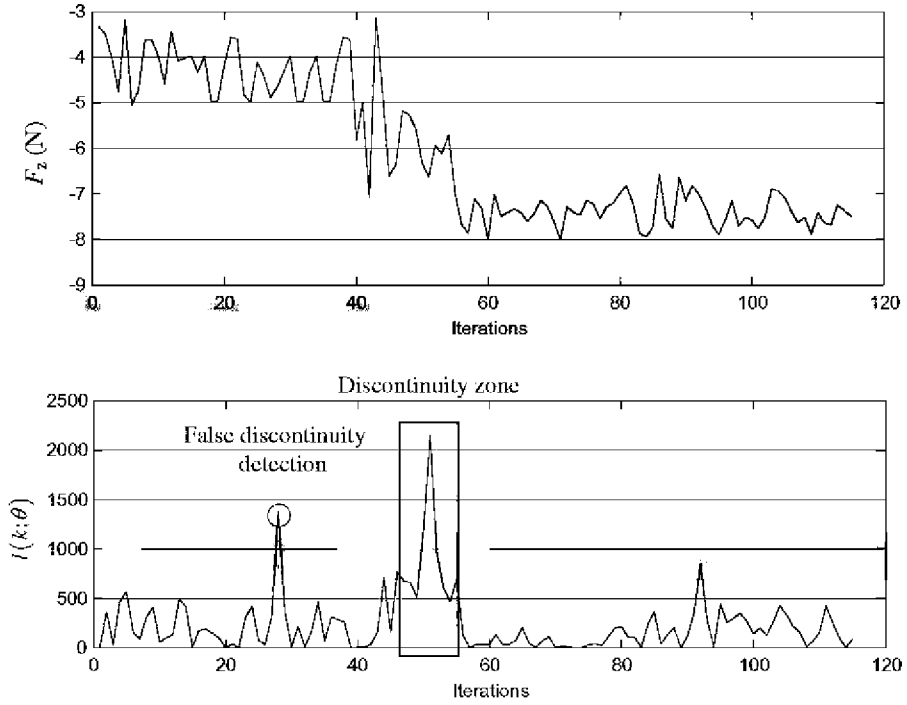

Fig. 16. Interaction forces and values of $l(k;\theta)$ during the tracking of a surface with a discontinuity. Experiment 2.

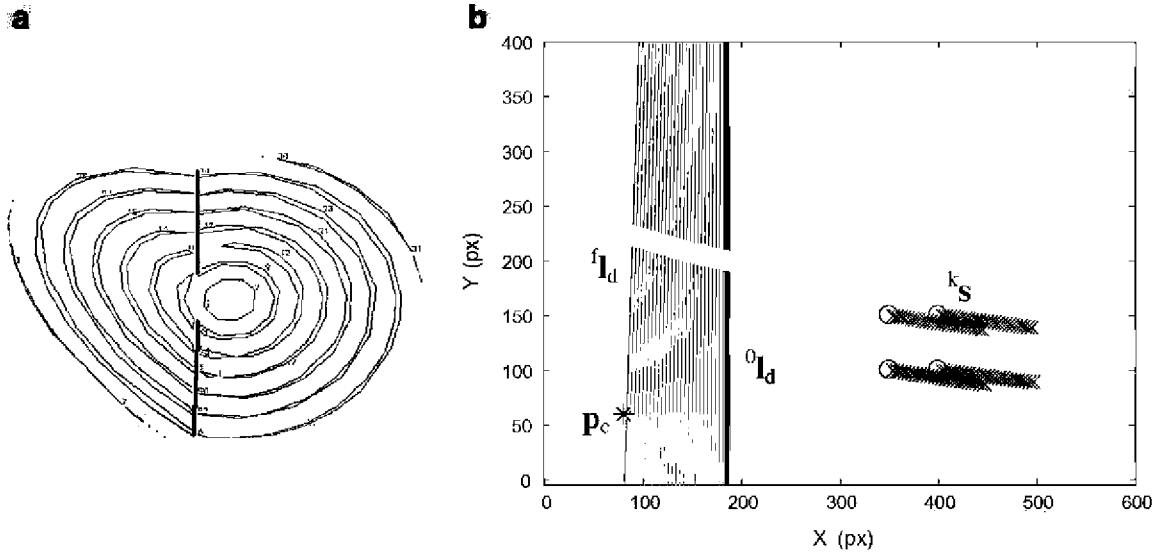

Fig. 17. (a) Zone of discontinuity using the method described in Section 4. (b) Process carried out to determine the point in which the end-effector arrives to the discontinuity. Experiment 2.

frictions or even the high noise level of the force sensor signal. To improve the detections we have included additional sensorial information from a laser. Using structured light, the system is able to automatically detect zones where the discontinuity can occur. Therefore, only the discontinuities determined by the force sensor which are near to the ones determined using structured light are considered to be correct.

Once the discontinuities are determined, now we are working in improving the surface recognition method in order to modify the image trajectory which is tracked by the visual servoing system depending on the information obtained from the force sensor.

Acknowledgements

This work was funded by the Spanish MCYT project "Diseño, Implementación y Experimentación de Escenarios de Manipulación Inteligentes para Aplicaciones de Ensamblado y Desensamblado Automático" (DPI2005-06222).

References

S. Hutchinson, G.D. Hager, P.I. Corke, A tutorial on visual servo control, IEEE Trans. Robot. Automat. 12 (5) (1996) 651–670.

J. Pagès, C. Collewet, F. Chaumette, J. Salvi, Robust decoupled visual servoing based on structured light, in: IEEE/RSJ International Conference on Intelligent Robots and Systems, IROS 2005, 2005, pp. 2676–2681.

D. Khadraoui, G. Motyl, P. Martinet, J. Gallice, F. Chaumette, Visual servoing in robotics scheme using a camera/laser-stripe sensor, IEEE Trans. Robot. Automat. 12 (5) (1996) 743–750.

A. Krupa, J. Gangloff, C. Doignon, M. Mathelin, G. Morel, J. Leroy, L. Soler, J. Marescaux, Autonomous 3d positioning of surgical instruments in robotized laparoscopic surgery using visual servoing, IEEE Trans. Robot. Automat. 19 (5) (2003) 842–853.

H. Bruyninckx, J. De Schutter, Specification of force-controlled actions in the task frame formalism-A synthesis, IEEE Trans. Robot. Automat. 12 (4) (1996) 581–589.

A. Namiki, I. Nakabo, M. Ishikawa, High speed grasping using visual–force feedback, in: IEEE International Conference on Robotics and Automation, Detroit, MI, 1999, pp. 3195–3200.

G. Morel, E. Malis, S. Boudet, Impedance based combination of visual–force control, in: IEEE International Conference on Robotics and Automation, Leuven, Belgium, 1998, pp. 1743–1748.

T. Tsuji, A. Hiromasa, M. Kaneko, Non-contact impedance control for redundant manipulators using visual information, in: IEEE International Conference on Robotics and Automation, Albuquerque, USA, vol. 3, 1997, pp. 2571–2576.

Y. Zhao, C. Cheah, Hybrid vision-force control for robot with uncertainties, in: Proceedings of IEEE International Conference on Robotics and Automation, 2004, pp. 261–266.

T. Olsson, R. Johansson, A. Robertsson, Flexible force-vision control for surface following using multiple cameras, in: Proceedings of IEEE/RSJ International Conference on Intelligent Robots and Systems, IROS 2004, 2004, pp. 798–803.

J. Pomares, F. Torres, Movement-flow based visual servoing and force control fusion for manipulation tasks in unstructured environments, IEEE Trans. Syst. Man and Cybernet. – Part C 35 (1) (2005) 4–15.

N. Hogan, Impedance control: an approach to manipulation: Part I-theory; part II-implementation; part III-applications, ASME J. Dyn. Syst. Meas. Control 107 (1985) 1–24.

D.E. Whitney, Force feedback control of manipulator fine motions, J. Dyn. Syst. Meas. Control (1977) 97.

Y. Mezouar, F. Chaumette, Path planning for robust image-based control, IEEE Trans. Robot. Automat. 18 (4) (2002) 534–549.

A.S. Willsky, H.L. Jones, A generalized likelihood ration approach to the detection and estimation of jumps in linear systems, IEEE Trans. Automat. Control 21 (1) (1976) 108–112.

O. Faugueras, F. Lustman, Motion and structure from motion in a piecewise planar environment, Int. J. Pattern Recognit. Artif. Intell. 2 (3) (1998) 485–508.

R. Behringer, Detection of discontinuities of road curvature by glr methods, in: Proceedings of International Symposium on Intelligent Vehicles. Detroit, USA, 1995.

P. Gil, F. Torres, O. Reinoso, A detection method of intersections for determining overlapping using active vision, in: International Conference on Computer Vision Theory and Applications, VISAPP 2006, vol. 1, 2006, pp. 501–507.

C.H. Teh, R.T. Chin, On the detection of dominant points on digital curves, IEEE Trans. PAMI 1 (8) (1989) 859–872.

D. Douglas, T. Peucker, Algorithms for the reduction of the number points required to represent a digitized line or its caricature, Can. Cartograph. 10 (2) (1973) 112–122.

J. Hershberger, J. Snoeyink, Speeding up the Douglas–Peucker line-simplification algorithm, in: Proceedings of 5th Symposium on Data Handling, 1993, pp. 134–143.

E. Chavez, G. Navarro, R. Baeza-Yates, J. Marroquín, Searching in metric spaces Technical Report TR/DCC-99-3, Department of Computer Science, University of Chile, 1999.

M.R. Teague, Image analysis via the general theory of moments, J. Opt. Soc. Am. 70 (8) (1980) 920–930.

R. Hartley, A. Zisserman, Multiple View Geometry in Computer Vision, Cambridge University Press, 2000, pp. 91–92.

S. Suzuki, K. Abe, Topological structural analysis of digital binary images by border following, Comput. Vis. Graph. Image Process. 30 (1) (1985) 32–46.

A. Handbury, Lexicographical order in the HLS colour space. Technical Report N-04/01/NM. Centre de Morphologie Mathematique Ecole des Mines de Paris, 2001.